THE ASTROPHYSICAL JOURNAL, 545:1089–1100, 2000 December 20

A MODEL FOR THE EMERGENCE OF A TWISTED MAGNETIC FLUX TUBE

D. W. LONGCOPE AND B. T. WELSCH
Department of Physics, Montana State University, Bozeman, MT 59717
Received 2000 April 28; accepted 2000 July 31

ABSTRACT

Observations have shown that active region flux tubes often emerge in a twisted state and that the active region formed has magnetic helicity of the same sense as the flux tube that forms it. Separate theoretical models have been developed for coronal magnetic fields with helicity and for flux tubes with twist. Here we present a dynamical model that connects a twisted subphotospheric flux tube to a force-free coronal field. With this model it is possible to explore the emergence of a flux tube into the corona and its effect on both the coronal field and the subphotospheric flux tube. In particular, the model shows that only a fraction of the current carried by the twisted flux tube will pass into the corona. As a consequence of this "mismatch," a torsional Alfvén wave is launched downward along the flux tube at the instant of emergence. As the flux tube continues to emerge, the helicity of the coronal field increases owing to rotation of the footpoints. Our model predicts that the level of rotation will depend upon the rapidity of flux emergence. After this transient period the helicity of the active region will reflect the twist in its parent tube.

Subject headings: MHD — Sun: activity — Sun: corona — Sun: magnetic fields

1. INTRODUCTION

Measurements of the full magnetic field at the Sun's photosphere show that, where magnetic field enters the corona, so does electric current. Evidence that at least some of the measured photospheric current passes into the corona is provided by the agreement between the shapes of coronal field lines, inferred from X-ray or EUV images, and model force-free fields (Pevtsov, Canfield, & McClymont 1997). Since currents "store" free magnetic energy, the importance of coronal currents was appreciated theoretically well before such modeling or measurements were done. This free energy may result in flaring in those active regions (ARs) with sheared photospheric fields and eruptions in those ARs with sigmoidal shapes (Canfield, Hudson, & McKenzie 1999).

A common approach to modeling current-carrying coronal fields is to anchor them in a dense lower layer—the photosphere. In such a model current may be generated by vortical motion of the photosphere, with no change in the net flux. Recent observations, however, show that actual current generation is somehow related to the emergence of new flux through the photosphere. Leka et al. (1996) found, in the emergence of AR 7260, that the total vertical current increased as the total (unsigned) flux did.

The prevailing picture of flux emergence is that an Ω-shaped flux tube pierces the photosphere after rising from the base of the convection zone (CZ). Dynamical models of slender isolated flux tubes have successfully reproduced many properties of observed bipolar ARs and sunspot pairs (Spruit 1981; Moreno-Insertis 1986; Choudhuri & Gilman 1987; Fisher, Chou, & McClymont 1989; Fan, Fisher, & McClymont 1994; Caligari, Moreno-Insertis, & Schüssler 1995). These models apply to a "thin" isolated tube of flux rising under its own buoyancy and impeded by aerodynamic drag. The flux tube is thin in the sense that its cross section is much smaller than the scales of the external atmosphere and is isolated in the sense that it is embedded in completely unmagnetized plasma. The degree of quantitative agreement between model and observation suggests that each assumption is approximately valid.

The Leka et al. observation, according to one interpretation, shows the emergence of a *twisted* magnetic flux tube—field lines within the tube twist about its axis (Longcope et al. 1999). A dynamical model of twisted magnetic flux tubes has been developed along similar lines to the models of untwisted tubes (Longcope & Klapper 1997). Solutions of the model equations have provided further evidence for pretwisted flux tubes by fitting observed AR chirality trends. A long-term study of AR fields had previously shown a slight latitude dependence in the vertical currents at the photosphere (Pevtsov, Canfield, & Metcalf 1995). Differential rotation acting on coronal fields would produce much smaller current (Longcope et al. 1999). Thin flux tube simulations, however, show that CZ turbulence with kinetic helicity will introduce twist in a rising flux tube (Longcope, Fisher, & Pevtsov 1998), whose magnitude and sign agree with observation.

For theoretical reasons it is necessary that isolated flux tubes be twisted in order to maintain their integrity (Schüssler 1979). Two-dimensional models show that hydrodynamic forces from the unmagnetized medium will quickly fragment an untwisted tube. Twist introduces an azimuthal magnetic field whose tension can counteract these hydrodynamic forces. This theoretical argument is evidently flawed in some respect since the amount of twist required to prevent fragmentation in a rising two-dimensional tube is at least 1 order of magnitude larger than values inferred from vector magnetic field measurements (Longcope et al. 1999). Such an observed discrepancy might arise if the current in the rising magnetic flux tube were not all passed into the corona.

In spite of the observational work discussed above, it is not well understood how the current in a subphotospheric flux tube couples to the field above it; indeed, the matter is the subject of controversy. According to some theories (Melrose 1991) a twisted flux tube carries a net current along its axis, like a household electrical wire. In this view a large self-inductance would prevent the current from changing during emergence or afterward. The large self-inductance comes from magnetic field created outside the

flux tube by its current. Indeed, a simple application of Faraday's law implies that the current-carrying flux tube cannot be isolated in truly field-free plasma. Requiring the flux tube's current to remain fixed places significant constraints on coronal dynamics, with implications for solar flares (Melrose 1997) and for transequatorial reconnection (Canfield, Pevtsov, & McClymont 1996; Pevtsov 2000). These constraints would not apply, however, if the subphotospheric current could leave the flux tube before entering the corona. This possibility has been a matter of some debate owing to the complex nature of the magnetic field near the photosphere.

On the other hand, if one insists that subphotospheric magnetic flux tubes are truly isolated (i.e., surrounded by field free plasma), then the above Faraday's law argument requires that they carry no net current. The twisted flux tube in a thin flux tube model therefore carries current inside, because of the twist, and an opposing return current on its surface. In spite of this clear theoretical requirement for a return current, photospheric measurements have never shown an AR with an opposing current surrounding it (Melrose 1991). It has been argued, however, that this is an effect of the measurements and does not imply a lack of flux confinement (Parker 1996).

The following work presents a model for the passage of subphotospheric currents into the corona. For magnetic fields of active region scale, say $\gtrsim 10$ Mm, the photospheric boundary is little more than an interface between low-β and high-β plasma. Existing thin flux tube models apply to regions of large β, where the tube may be confined by plasma pressure. Force-free coronal models, on the other hand, assume a low-β plasma completely filled with magnetic field. The work presented here joins the two types of model across a photospheric interface. Considering large-scale forces and the motions they drive, we arrive at a scenario for the emergence of a twisted magnetic flux tube.

The resulting model clarifies several elements in the relationship between subphotospheric and coronal currents. First of all, the surface current from a flux tube need not enter the corona, nor would it be necessarily evident in vector magnetic field measurements made of the photosphere. Second, the twist observed in the photospheric field is not always representative of the twist in the subphotospheric flux tube. During the emergence and a transient period thereafter, only a fraction of the tube's current enters the corona. With time this current mismatch diminishes, and the coronal twist increases to match the twist of the flux tube.

The combined flux tube/AR model will be presented and analyzed as follows. In the next section we present models for a force-free coronal field, a thin twisted flux tube, and then for the interface connecting them. The following section, § 3, applies the combined model to the emergence of a twisted magnetic flux tube. Finally, § 4 discusses the implications of this model for the issues described above: the passage of current from the CZ to the corona, and the relation of measured twist to the twist in the rising flux tube.

2. THE MODEL

For simplicity, our model assumes axisymmetry for both the flux tube and the active region fields. Working in cylindrical coordinates (ϖ, ϕ, z) the general magnetic field can be written in terms of a flux function $f(\varpi, z)$

$$\boldsymbol{B}(\varpi, z) = \nabla f \times \nabla\phi + \varpi B_\phi(\varpi, z)\nabla\phi \ , \tag{1}$$

whose contours define flux surfaces. The magnetic field takes the form of an isolated flux tube in the high-β CZ and a more extended active region field in the low-β corona. In our axisymmetric model the corona will be represented by the slab $-d < z < d$ while the region outside this, $|z| > d$, is the CZ (see Fig. 1). The two planes $z = \pm d$ separating the corona from the CZ (i.e., where β changes discontinuously) will be called the photosphere. Each plane actually represents many scale heights of the solar atmosphere where β changes from very large to very small. Across this boundary we apply only integral constraints that are equivalent to those for a thin layer of finite extent. We quantify this aspect of the model below.

In the CZ, $|z| > d$, the flux Φ is confined to a tube of radius a by a slight excess in the large pressure of the unmagnetized plasma around it. The magnetic field profile $B_z(\varpi)$ is arbitrary within the tube because of the large value of β: any radial magnetic forces are balanced by pressure gradients. For added simplicity we will assume uniform field strength within this cylinder,

$$f = \Phi\varpi^2/2\pi a^2 \ . \tag{2}$$

The flux tube's magnetic field is discussed in more detail in § 2.2.

In the corona, $|z| < d$, the plasma pressure is insufficient to confine the flux, which therefore expands into a volume we will call the *active region*. The active region consists of all the magnetic flux from the flux tube passing between $z = -d$ and $z = d$. Our calculations will admit the possibility of currents flowing within the active region field. Outside of the active region is current-free flux not anchored to the photosphere. This is the corona's "vacuum field," intended to represent the preexisting flux into which the active region emerges. The active region is separated from the vacuum field by an interface defined by the curve $\varpi = \varpi_s(z)$, whose location will be determined self-consistently along with the active region field.

2.1. *The Corona*

Lacking a significant contribution from the plasma pressure, magnetic forces will drive the coronal plasma toward a state of minimum magnetic energy. The magnetic energy is

$$E_M = \frac{1}{8\pi}\int |\boldsymbol{B}|^2 d^3\boldsymbol{x} = \frac{1}{4}\int_{-d}^{d} dz \int_0^R \varpi\, d\varpi \left(\frac{1}{\varpi^2}\,|\nabla f|^2 + B_\phi^2\right), \tag{3}$$

where a large outer radius, $R \gg d$, is introduced to make this quantity finite. We assume that this energy minimization completely determines the form of the coronal magnetic field. Severe constraints are placed on the plasma motions by the large conductivity of the coronal plasma unless one admits the possibility of magnetic reconnection.

It is well known that magnetic reconnection will eliminate all of the aforementioned constraints except for total helicity and total flux (Woltjer 1958; Taylor 1974). This leaves both functions, $f(\varpi, z)$ and $B_\phi(\varpi, z)$, free to minimize expression (3), subject only to two integral constraints and boundary conditions. To maintain $\nabla \cdot \boldsymbol{B} = 0$ the normal component of the magnetic field must be continuous across

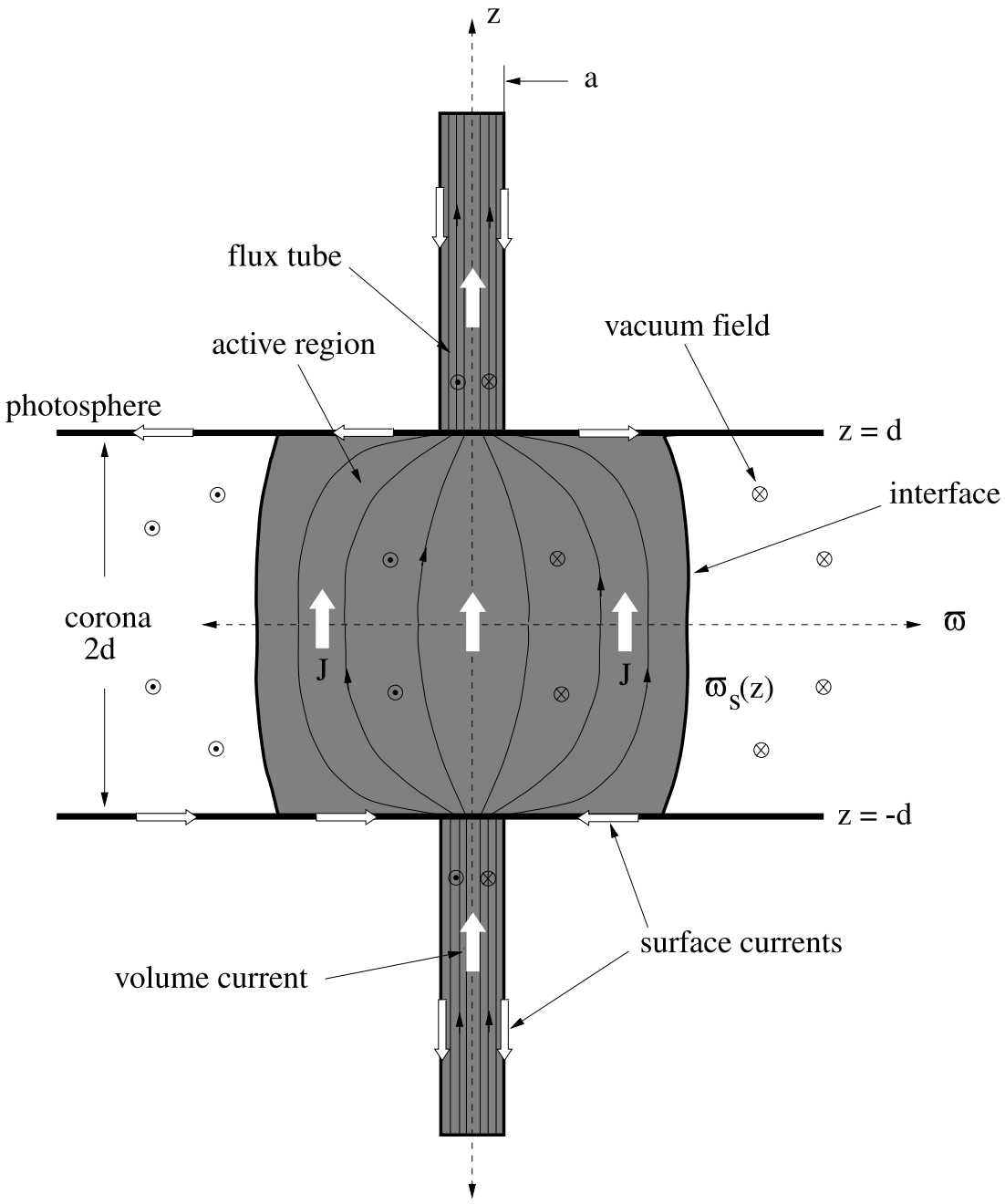

FIG. 1.—Geometry for the flux tube and active region magnetic fields

the photospheric boundary. This fixes f at $z = \pm d$, with the Dirichlet boundary condition

$$f(\varpi, z = \pm d) = \begin{cases} \Phi\varpi^2/2\pi a^2 & \varpi \le a, \\ \Phi/2\pi & \varpi > a. \end{cases} \tag{4}$$

The integral constraints on the minimization are the total helicity and the total flux, neither of which can be changed by plasma motion even during episodes of fast reconnection. Since our active region field lines cross the boundaries at $z = \pm d$, it is actually the *relative helicity* (Berger & Field 1984; Finn & Antonsen 1985) that is constant. This is a specific form of the conventional magnetic helicity $\int \boldsymbol{A} \cdot \boldsymbol{B} \mathrm{d}^3x$, which is gauge invariant even when flux crosses the boundary. Inside the active region, $\varpi < \varpi_s(z)$, we define a potential (i.e., current-free) magnetic field $\boldsymbol{B}_p$ with the same normal components as $\boldsymbol{B}$. In terms of this field, and its vector potential $\boldsymbol{A}_p$, the relative helicity can be written (Finn & Antonsen 1985; Berger 1999)

$$H_{\mathrm{ar}} = \int (\boldsymbol{A} + \boldsymbol{A}_p) \cdot (\boldsymbol{B} - \boldsymbol{B}_p) d^3x = 4\pi \int_{-d}^{d} dz \int_0^{\varpi_s(z)} f B_\phi \, d\varpi \, . \tag{5}$$

The second constraint is the total toroidal flux in the vacuum field,

$$\Psi_v = \int_{-d}^{d} dz \int_{\varpi_s(z)}^{R} B_\phi \, d\varpi \, . \tag{6}$$

The outer radius R is taken to be so large that the vacuum field will function as a virtually inexhaustible reservoir of flux. In spite of this, it is still formally necessary to impose constraint (6) to obtain a well-defined minimization.

Performing the constrained variations, with Lagrange multipliers $\alpha/8\pi$ on equation (5) and $\lambda/2$ on equation (6), yields Euler-Lagrange equations

$$\varpi B_\phi = \alpha f$$
$$\frac{\partial}{\partial \varpi}\left(\frac{1}{\varpi}\frac{\partial f}{\partial \varpi}\right) + \frac{1}{\varpi}\frac{\partial^2 f}{\partial z^2} = -\alpha B_\phi \tag{7}$$

for $\varpi < \varpi_s(z)$,

$$\varpi B_\phi = \lambda$$
$$\frac{\partial}{\partial \varpi}\left(\frac{1}{\varpi}\frac{\partial f}{\partial \varpi}\right) + \frac{1}{\varpi}\frac{\partial^2 f}{\partial z^2} = 0 \tag{8}$$

for $\varpi > \varpi_s(z)$. Taken together, the equations for the active region, equation (7), yield the linear Grad-Shafranov equation

$$\varpi \frac{\partial}{\partial \varpi}\left(\frac{1}{\varpi}\frac{\partial f}{\partial \varpi}\right) + \frac{\partial^2 f}{\partial z^2} = -\alpha^2 f, \quad \varpi < \varpi_s(z) \tag{9}$$

describing a constant-α force-free field.

The energy integral must also be minimized under variations of the interface $\varpi_s(z)$, subject to the same integral constraints on helicity and flux. The resulting Euler-Lagrange equation at the point of interface is

$$-\frac{1}{4}\left[\frac{1}{\varpi}|\nabla f|^2 + \varpi B_\phi^2\right]_{\varpi_s} - \frac{1}{2}\alpha f B_\phi|_{\varpi_s -} + \frac{1}{2}\lambda B_\phi|_{\varpi_s +} = 0\,, \tag{10}$$

where $[\,\cdot\,]_{\varpi_s}$ is the discontinuity across the interface (outside minus inside). Using equations (7) and (8), this can be written in the simpler form

$$\left[\varpi^{-2}|\nabla f|^2\right]_{\varpi_s} - \left[B_\phi^2\right]_{\varpi_s} = 0\,. \tag{11}$$

This expression is notably different from the requirement of magnetic pressure balance across the interface,

$$\left[\varpi^{-2}|\nabla f|^2\right]_{\varpi_s} + \left[B_\phi^2\right]_{\varpi_s} = 0\,, \tag{12}$$

which follows from an *unconstrained* variation of equation (3).

To be in force balance across the interface, and a minimum energy subject to constraints, the equilibrium must satisfy both equations (11) and (12). The combination is equivalent to the condition that $|\nabla f|$ and $|B_\phi|$ be continuous across $\varpi_s(z)$. Since the interface is defined to be the outer boundary of the flux from the tube, it must occur at $f(\varpi_s, z) = \Phi/2\pi$. Thus, at the interface $f(\varpi, z)$ must satisfy

$$f(\varpi = \varpi_s, z) = \frac{\Phi}{2\pi}\,, \tag{13}$$

$$\left|\frac{\partial f}{\partial \varpi}\right|_{\varpi = \varpi_s} = 0\,. \tag{14}$$

Among other things this means that no surface current flows along the AR/vacuum interface. While such a surface current might be consistent with strict force balance (12), it is not the equilibrium with minimum magnetic energy.

The boundary conditions on $f(\varpi, z)$ in the vacuum admit only the trivial solution $f = \Phi/2\pi$. This means that the vacuum field is purely toroidal, with

$$B_\phi = \frac{\alpha\Phi}{2\pi}\frac{1}{\varpi}\,, \quad \varpi > \varpi_s(z)\,. \tag{15}$$

This is the field from the axial current $I = \alpha\Phi$ (cgs-emu), flowing along the active region field. This net current is another manifestation of the lack of return current at the interface.

2.2. *The Flux Tube*

In the high-β region "below" the photosphere ($|z| > d$) the flux tube is confined to radius a and assumed to have uniform axial field strength B_z. The flux tube consists of twisted field lines, whose azimuthal field strength can be written in terms of the pitch q,

$$B_\phi = \varpi q B_z\,. \tag{16}$$

Positive q defines field pitched in right-handed helices, wrapping once about the axis over the axial distance $2\pi/q$. We will assume that the field line pitch is uniform across the tube's profile, so q is independent of ϖ (this is a natural assumption if the twist was introduced by a motion of the flux tube; Linton, Longcope, & Fisher 1996; Longcope, Fisher, & Pevtsov 1998). The uniform twist implies a uniform axial current density $\boldsymbol{J} = 2qB_z\hat{\boldsymbol{z}}$ whose total current (in cgs-emu) is $I = 2q\Phi$. The flux tube is surrounded by unmagnetized plasma and does not, therefore, carry a net current. There is, per force, an axial surface current flowing along the outside of the tube $\varpi = a$, canceling the axial volume current from the twist (see Fig. 1).

It is worth noting that, while there is a surface current at $f = \Phi/2\pi$ in the CZ, the analysis of the previous section shows such a surface current to be absent from the corona. The difference stems from β: the large plasma pressure in the CZ can balance the stresses of a surface current sheet, while the meager plasma pressure in the corona cannot. This means that the flux tube's surface current cannot enter the corona; it must continue along the photosphere at $z = \pm d$, as shown in Figure 1. This is an important feature of the model; however, it arises mostly from kinematic considerations. We discuss more of its consequences below.

While the pitch of the flux tube is uniform over each cross section, it may vary along the axis, $q(z)$. This variation in twist implies a radial current density

$$J_r = \frac{\partial B_\phi}{\partial z} = \varpi B_z \frac{\partial q}{\partial z}\,. \tag{17}$$

Radial current crosses the axial magnetic field giving rise to an azimuthal force $F_\phi = -J_r B_z$; this is a magnetic torque. While gradients in the internal plasma pressure can easily balance radial magnetic forces, they cannot create torque. Thus, the total torque on a section of the tube is (Longcope & Klapper 1997)

$$\tau \equiv \frac{1}{4\pi}\oint (\boldsymbol{r}\times\boldsymbol{B})(\boldsymbol{B}\cdot\hat{\boldsymbol{n}})dS\,, \tag{18}$$

independent of pressure. On a short interval $(z, z + dz)$ the only contributions to this integral come from its end sections

$$\boldsymbol{M}(z) = \tfrac{1}{2} B_z \hat{\boldsymbol{z}} \int_0^a B_\phi \varpi^2 \, d\varpi = \tfrac{1}{8} q(z) a^4 B_z^2 \hat{\boldsymbol{z}} \, . \tag{19}$$

The torque on the small tube section is therefore purely axial,

$$\tau_z = \frac{\partial M_z}{\partial z} \, dz = \frac{1}{8} \, a^4 B_z^2 \, \frac{\partial q}{\partial z} \, dz \, . \tag{20}$$

A consequence of expression (20) is that to be in equilibrium ($\tau = 0$) the tube's twist cannot vary along its axis, $\partial q/\partial z = 0$. This is equivalent to a requirement that the axial volume current $I = 2q\Phi$ pass uninterrupted along the axis. The alternative, a change in the axial volume current, means that current must be shunted radially to join the surface current, since $\nabla \cdot \boldsymbol{J} = 0$. This shunting is the same radial current that gives rise to the axial torque τ_z discussed above. Thus, our model permits the flux tube's current I to change, but doing so gives rise to torque.

A net axial torque will cause the section of the tube to spin about its axis. We will assume the spinning motion to be rigid $v_\phi = \varpi\omega$ (this is required for consistency with the previous assumption that q did not vary across the tube). The angular momentum of a spinning tube section is

$$L_z = \int \rho \varpi v_\phi \, dV = \tfrac{1}{2} \pi a^4 \rho \omega \, dz \, , \tag{21}$$

where ρ is the mass density of the CZ plasma. Thus, the torque τ_z will change the local spin rate

$$\frac{\partial \omega}{\partial t} = v_{\rm A}^2 \, \frac{\partial q}{\partial z} \, , \tag{22}$$

where $v_{\rm A} = B_z/(4\pi\rho)^{1/2}$ is the Alfvén speed in the CZ.

A second relation between q and ω is provided by helicity considerations (Longcope & Klapper 1997). The relative helicity of the tube section is

$$H = 4\pi \, dz \int_0^a f B_\phi \, d\varpi = \frac{\Phi^2}{2\pi} \, q \, dz \, . \tag{23}$$

This quantity is constant only so long as those boundaries through which field lines pass remain fixed. Rigid rotation of the cross sections will change the helicity (Berger 1999)

$$\frac{dH}{dt} = \oint (\boldsymbol{B} \cdot \hat{\boldsymbol{n}}) \boldsymbol{v} \cdot (\boldsymbol{A} + \boldsymbol{A}_p) dS = \frac{\Phi^2}{2\pi} \, \frac{\partial \omega}{\partial z} \, dz \, . \tag{24}$$

Setting this equal to the time derivative of expression (23) gives an equation for the evolution of q,

$$\frac{\partial q}{\partial t} = \frac{\partial \omega}{\partial z} \, . \tag{25}$$

(We have assumed that the length of the tube section, dz, remains constant). This and equation (22) form a set of telegrapher's equations, whose solutions are leftward and rightward propagation torsional Alfvén waves (Priest 1982).

2.3. *The Photosphere*

The goal of this work is to model the interaction of the twisted flux tube with the coronal field. The corona is here modeled as force free; however, force-free magnetic fields always exert stresses on their boundaries. In this case the coronal field stresses the photospheric boundaries radially at $z = \pm d$. The much larger pressures at the photosphere are capable of balancing large stresses; however, they cannot balance azimuthal forces or torques. The net torque on the footpoint $z = -d$ can be found using expression (18) on a dome of radius $s \gg a$ extending into the corona (see Fig. 2*a*)

$$\tau_z = \frac{1}{2} \, s^3 \int_0^{\pi/2} (\hat{\boldsymbol{z}} \cdot \hat{\boldsymbol{r}} \times \hat{\boldsymbol{\phi}}) B_\phi \, B_r \, \sin\theta \, d\theta - \frac{\Phi^2}{8\pi^2} \, q(-d) \, .$$

The first term comes from the hemisphere D in the corona, the second term from its flat base C located just below the photosphere. Using equation (9) for the coronal field gives $B_\phi = \alpha f/s \, \sin\theta$ and

$$\tau_z = \frac{\alpha}{2} \int_0^{\pi/2} f \, \frac{\partial f}{\partial \theta} d\theta - \frac{\Phi^2}{8\pi^2} \, q(-d) = \frac{\Phi^2}{16\pi^2} \, [\alpha - 2q(-d)] \, . \tag{26}$$

Since coronal plasma in the dome has significantly less inertia than the CZ plasma beneath the base, there will be little opportunity for a torque imbalance at the interface. Setting (26) to zero, and similarly for the $z = d$ footpoint, gives the requirement

$$q(d) = q(-d) = \tfrac{1}{2}\alpha \, . \tag{27}$$

This means that the entire volume current from the flux tube must pass into the corona. The return current, on the tube's outer boundary, *does not* pass into the corona, leaving an unneutralized current $I = \alpha\Phi$ there.

Allowing for a photospheric layer of small but finite thickness δ (Fig. 2*b*) changes this result only slightly. The net torque on the photospheric tube section follows from expression (26)

$$\tau_z = \frac{\Phi^2}{16\pi^2} \, [\alpha - 2q(-d - \delta)] = \frac{\Phi^2}{8\pi^2} \, \Delta q \, , \tag{28}$$

where $\Delta q = \alpha/2 - q(-d - \delta)$ is the twist mismatch across the photosphere. Setting this equal to the change in angular momentum of the photospheric tube element (taken to be a cone),

$$\Delta q = \frac{8\pi^2}{\Phi^2} \, \frac{\pi}{10} \, \rho_{\rm ph} r^4 \delta \, \frac{d\omega}{dt} = \frac{4}{5} \, \frac{\delta}{v_{\rm A,\,ph}^2} \, \frac{d\omega}{dt} \, , \tag{29}$$

where $v_{\rm A,\,ph}$ is the average Alfvén velocity in the interface layer.

It follows from equation (22) that a disturbance of wavelength λ propagating on the tube will spin up the interface at

$$\frac{d\omega}{dt} \sim \frac{v_{\rm A}^2 \, q}{\lambda} \, , \tag{30}$$

where q and $v_{\rm A}$ characterize the CZ flux tube. Using this in expression (29) gives

$$\frac{\Delta q}{q} \sim \frac{\delta}{\lambda} \, \frac{v_{\rm A}^2}{v_{\rm A,\,ph}^2} \, . \tag{31}$$

We expect $v_{\rm A} < v_{\rm A,\,ph}$ since the Alfvén speed generally decreases with increasing depth. Thus, for disturbances much longer than the thickness of our photospheric layer

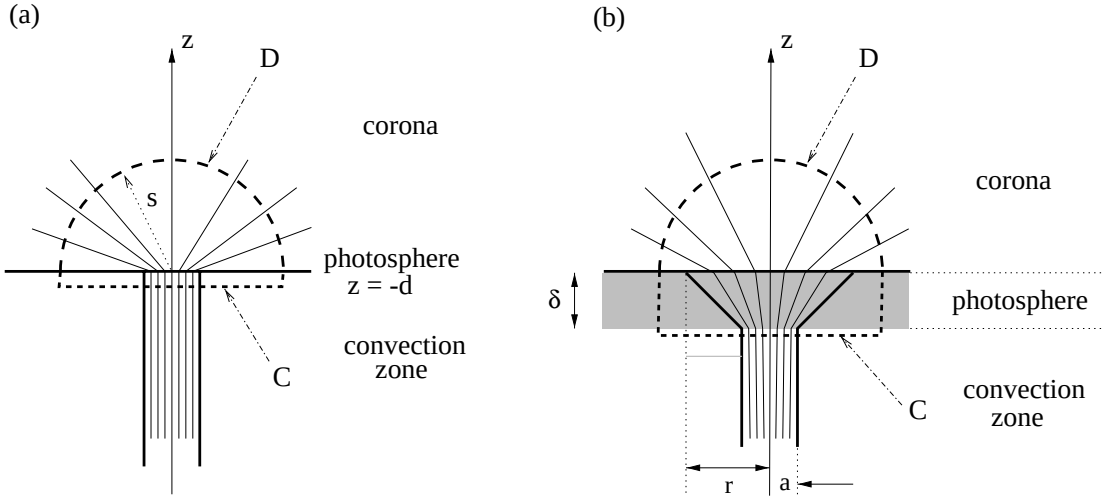

FIG. 2.—Hemispheric surface used to calculate the torque balance at the photosphere. Surface D is a hemisphere of radius $s \gg a$ the radius of the flux tube. Surface C is a flat end section located below the photosphere. Cases with photospheres of (*a*) zero thickness and (*b*) finite thickness δ give similar results.

$\lambda \gg \delta$ we find that $\Delta q \ll q$ and torque balance in expression (27) holds to leading order.

This consideration has shown the photospheric layer to be so thin and so light that it permits the shunting of axial currents only for short times. Taking a photospheric layer $\delta = 10$ Mm thick (i.e., the region over which flux tubes cannot be considered truly thin), significant torque imbalances cannot last longer than $\delta/v_A \simeq 3$ hr. On timescales much longer than this, those which interest us, the photosphere is dynamically equivalent to a genuine interface between the CZ and the corona. Hereinafter we return to this simpler picture and take $\delta = 0$.

As viewed from the corona, the rigid spinning of the footpoints will change the helicity of the active region. Applying expression (24) to the corona

$$\frac{dH_{\rm ar}}{dt} = \frac{\Phi^2}{2\pi}\left[\omega(d) - \omega(-d)\right] . \tag{32}$$

Differential spin between the two footpoints will thereby change the active region's helicity. This will in turn change the constraint on the force-free equilibrium, thus changing the value of α. To simplify the model we will assume that coronal relaxation occurs on timescales much shorter than this helicity change. The corona will evolve quasi-statically through a series of force-free equilibria characterized by time-dependent α.

3. APPLICATION TO AN EMERGING FLUX TUBE

3.1. *The Coronal Solution*

The evolution of the twisted flux tube depends on the response of the coronal fields. This response is entirely contained in the expression for the active region's helicity $H_{\rm ar}$. The helicity depends, in turn, on the solution to the Grad-Shafranov equation (9). Taking the limit that the flux tube radius is very small, $a \to 0$, the solution to equation (9) can be written in terms of a rescaled function

$$f(\varpi, z) = \frac{\Phi}{2\pi} F(\varpi/d, z/d; \alpha d) . \tag{33}$$

The rescaled function $F(x, y; \gamma)$ satisfies the same Grad-Shafranov equation

$$x \frac{\partial}{\partial x}\left(\frac{1}{x}\frac{\partial F}{\partial x}\right) + \frac{\partial^2 F}{\partial y^2} = -\gamma^2 F , \tag{34}$$

for the region inside the interface $x < x_s(y)$. This forms a free surface for the solution of equation (34). The solution is subject to the four boundary conditions

$$F(x = 0, y) = 0, \qquad \text{I}$$

$$F(x, y = \pm 1) = 1, \qquad \text{II}$$

$$F(x = x_s, y) = 1, \qquad \text{III}$$

$$\left.\frac{\partial F}{\partial x}\right|_{x = x_s} = 0, \qquad \text{IV} .$$

A numerical method for solving equation (34) is presented in the Appendix. Examples of $F(x, y)$ at values $\gamma = 0.5$ and $\gamma = 1.5$ are shown in Figures 3*a* and 3*b*. The outermost contour, $x_s(y)$, marks the outside of the active region. Smaller currents γ result in more expansive surfaces x_s. A potential field, $\gamma = 0$, would fill the corona entirely, $x_s = \infty$.

Once the dimensionless flux function $F(x, y; \gamma)$ is found, the active region's helicity can be calculated

$$H_{\rm ar} = 4\pi\alpha \int_{-d}^{d} dz \int_0^{\varpi_s(z)} f^2 \frac{d\varpi}{\varpi} = \frac{\Phi^2}{2\pi} h(\alpha d) , \tag{35}$$

where the dimensionless helicity function is defined

$$h(\gamma) \equiv 2\gamma \int_{-1}^{1} dy \int_0^{x_s(y)} F^2 \frac{dx}{x} . \tag{36}$$

It is shown below that the derivative of this function entirely dictates the dynamical interaction of the flux tube with the corona. Both $h(\gamma)$ and $h'(\gamma)$ are shown in Figure 3.

3.2. *Emergence*

The emergence of a flux tube into the corona will be modeled here by increasing the footpoint separation d. The photospheric boundaries at $z = \pm d$ move apart; however, we will assume that no plasma flows across these moving

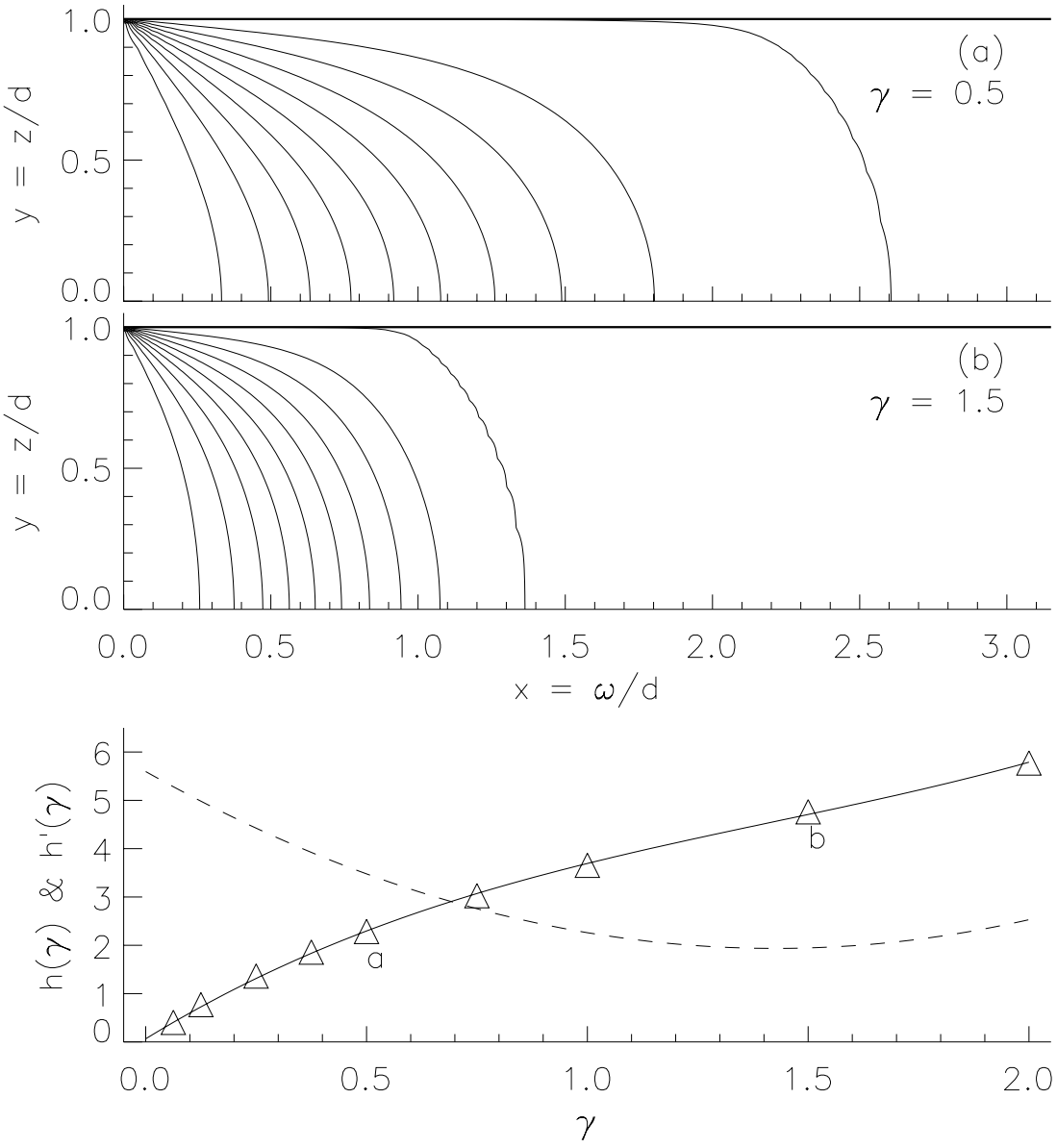

FIG. 3.—Solution of the Grad-Shafranov equation for $F(x, y)$. (*a*) Contours of $F(x, y)$ with $\gamma = 0.5$ plotted vs. $x = \varpi/d$ and $y = z/d$. Contours levels shown are $F = 0.1, 0.2, 0.3, \ldots 0.9, 0.999$; the final contour level is the numerical approximation to the interface $x_s(y)$. (*b*) Same as (*a*) but with $\gamma = 1.5$. (*c*) Plots of helicity $h(\gamma)$ (*solid curve*) and its derivative $h'(\gamma)$ (*dashed curve*). Triangles indicate the values of γ at which $F(x, y)$ was calculated.

planes. Flux emerging into the real corona is observed to drain very rapidly. It is this rapid draining we wish to model with the impenetrable surfaces $z = \pm d(t)$. To treat the separation more simply we adopt comoving coordinates $\zeta = z \mp d(t)$, for z to the right/left of the corona. The telegrapher's equations remain unchanged in the new coordinates,

$$\frac{\partial q}{\partial t} = \frac{\partial \omega}{\partial \zeta} \tag{37}$$

$$\frac{\partial \omega}{\partial t} = v_A^2 \frac{\partial q}{\partial \zeta}, \tag{38}$$

even as the separation d changes.

The point $\zeta = 0$ represents the entire corona, while the footpoints $z = \pm d$ are $\zeta = 0^{\pm}$. Equation (27) shows that $q(\zeta)$ is continuous across $\zeta = 0$ with $q(0) = q_0 = \frac{1}{2}\alpha$. Equation (32) implies, however, that the spin rate ω has a discontinuity across $\zeta = 0$

$$[\omega] = \frac{dh}{dt} = 2(d\dot{q}_0 + q_0 \dot{d})h'(2q_0 d) . \tag{39}$$

We begin with a flux tube in equilibrium, having uniform twist $q = q_\infty$. Emergence then begins as $d(t)$ increases from zero at $t = 0$. Torsional Alfvén waves resulting from this process will travel away from $\zeta = 0$. We can write the outward traveling solution to equations (37) and (38) in terms of a dimensionless shape function $s(t)$ (eq. [38])

$$q(\zeta, t) = q_\infty s(t - |\zeta|/v_A) , \tag{40}$$

$$\omega(\zeta, t) = v_A q_\infty \text{ sgn } (\zeta)[1 - s(t - |\zeta|/v_A)] . \tag{41}$$

Replacing this solution into equation (39) provides an equation determining the pulse shape $s(t)$ in terms of the emergence history $d(t)$

$$\frac{ds}{dt} = -s\frac{\dot{d}}{d} + \frac{v_A}{h'(2q_\infty sd)}\frac{1-s}{d}. \tag{42}$$

The entire history of the corona and the flux tube are found by solving this single ordinary differential equation for $s(t)$. As a demonstration we consider poles that start together at $t = 0$ and exponentially approach a final separation d_0 over the emergence time t_e,

$$d(t) = d_0(1 - e^{-t/t_e}). \tag{43}$$

Figure 4 shows a case of rapid emergence, $t_e = 0.5d_0/v_A$, while Figure 5 shows a slow emergence $t_e = 5d_0/v_A$. The solutions $s(t)$, the solid curves along the bottom, show the typical behavior of the model: coronal current increases toward a final value. The coronal equilibrium approaches the solution with $\gamma = 2q_\infty d_0 \equiv \gamma_\infty$. Each of the cases shown has $\gamma_\infty = 1.6$.

During the initial phase of emergence the flux tube's twist is suppressed by a fraction

$$s(0) = \frac{1}{1 + h'(0)\dot{d}(0)/v_A}. \tag{44}$$

This suppression factor can be significantly smaller than unity in a rapid emergence where $\dot{d} \gg v_A$, as it is in Figure 4. After emergence is complete, $\dot{d} = 0$, the flux tube returns to its initial twist $q = q_\infty$ as $s \simeq 1 - e^{-t/\tau}$, where the characteristic relaxation time is

$$\tau \equiv \frac{d_0 h'(\gamma_\infty)}{v_A}. \tag{45}$$

The relaxation time is roughly $\tau_A \equiv d_0/v_A$, the time a torsional Alfvén wave below the photosphere takes to travel the separation distance d_0. For $v_A = 10^5$ cm s^{-1} and $d = 10^{10}$ cm, the characteristic relaxation time is roughly 1 day. The actual relaxation time τ is longer than τ_A by a factor $h'(\gamma_\infty)$, which is ~ 6 in Figure 4.

Contours for $F(x, y)$ from three successive times are shown in Figures as insets (*a*), (*b*), and (*c*) of Figures 4 and 5.

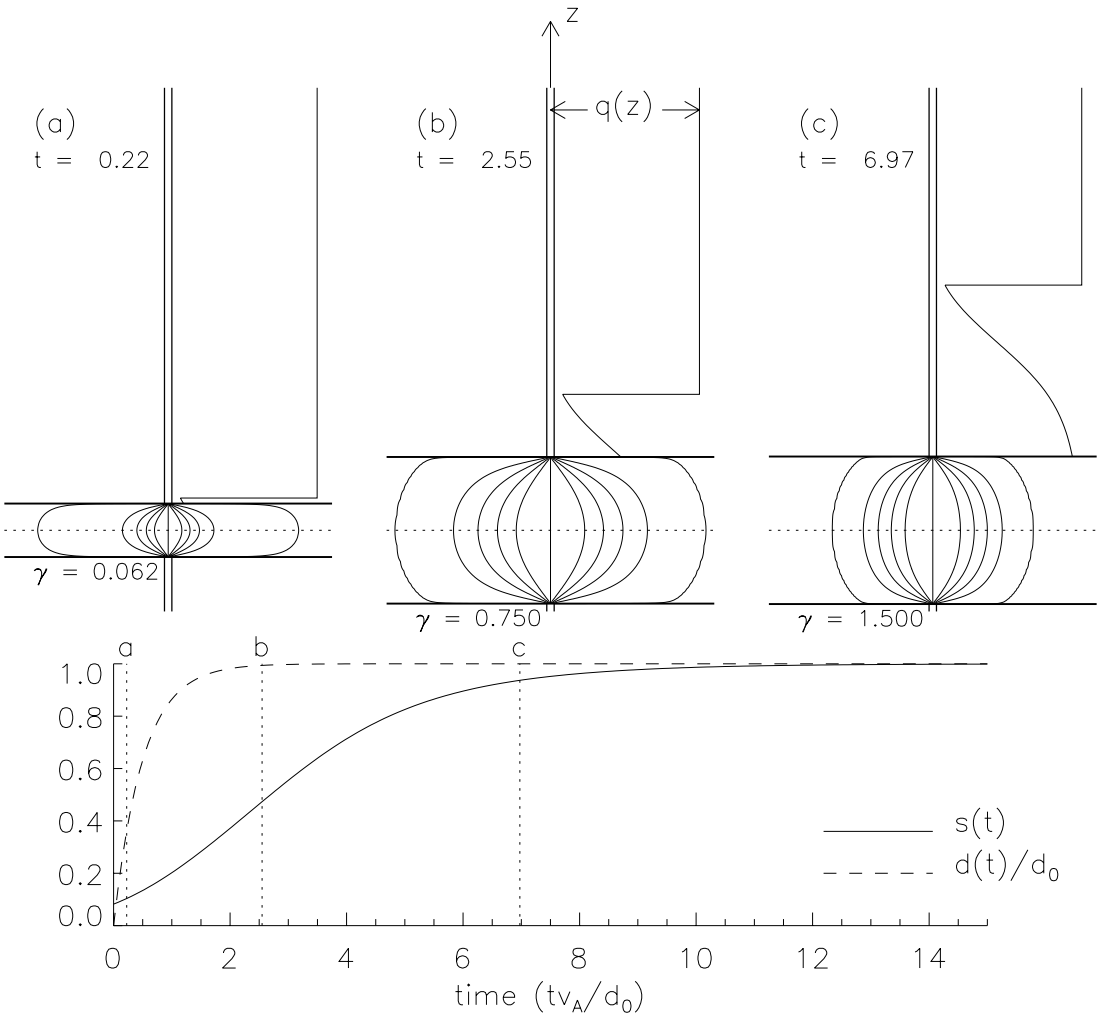

FIG. 4.—Rapid emergence of a flux tube. Emergence time is $t_e = 0.5d_0/v_A$, and final twist is $\gamma_\infty = 2q_\infty d_0 = 1.6$. The solution $s(t)$ is shown as a solid curve and separation $d(t)/d_0$ as a dashed curve along the bottom. *Top:* Coronal equilibria $F(x, y)$ are shown at times (*a*) $t = 0.22$, (*b*) 2.55, and (*c*) 6.97. The locations of these snapshots in the time history are shown by vertical dotted lines. The propagating twist pulse $q(z)$ is shown along each of the flux tubes in the snapshots.

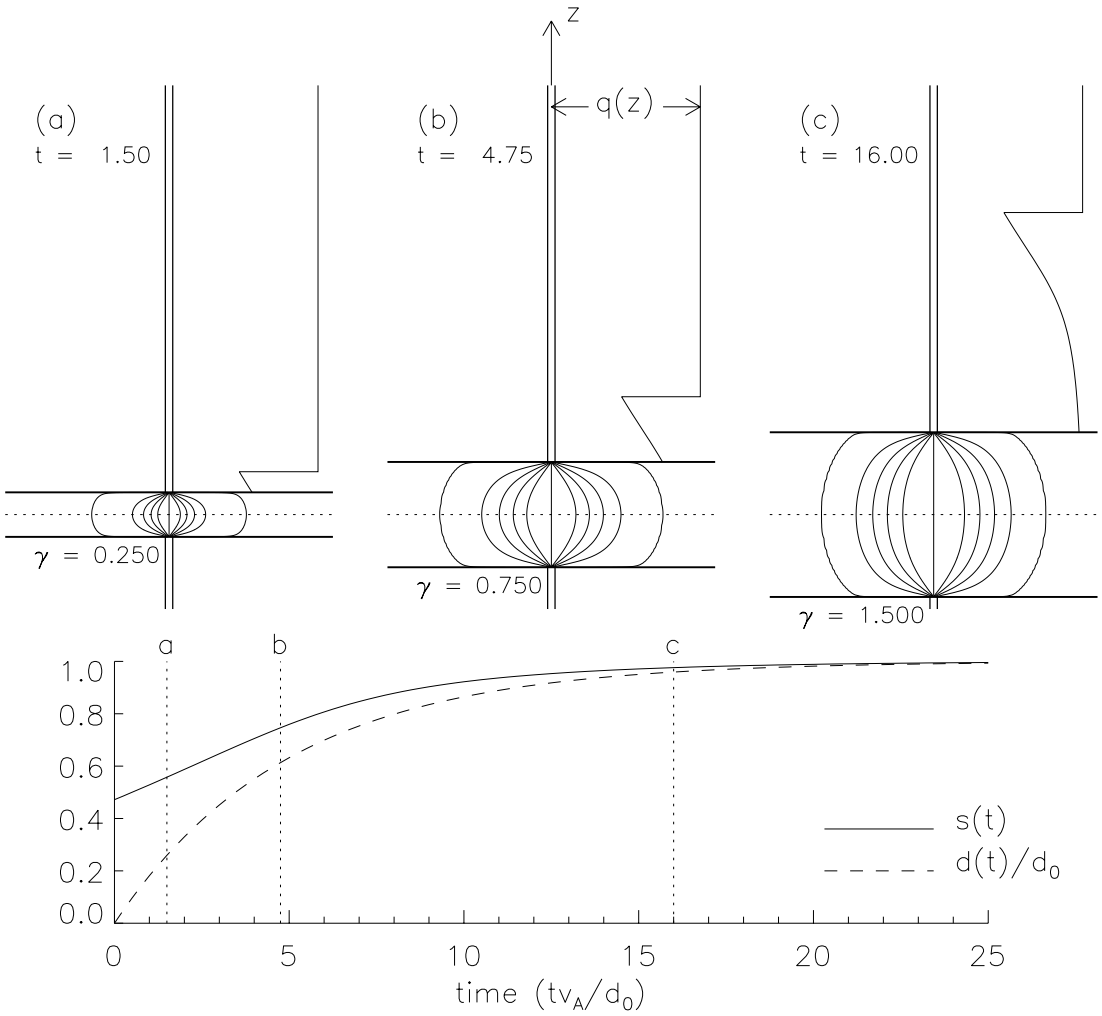

FIG. 5.—Slow emergence of a flux tube. Same format as Fig. 4 except that $t_e = 5d_0/v_A$.

These show the equilibrium pinching toward the axis as the coronal current (i.e., α) increases. Initially, the decreasing radius is compensated for by an increasing separation $d(t)$.

Evolution of the coronal field launches torsional Alfvén pulses upward ($v > 0$) and downward ($v < 0$) along the flux tube. The upward propagating pulse is shown in insets (*a*), (*b*), and (*c*). The pulses are a rarefaction in twist $q(z)$ from its equilibrium value q_∞. The pair of twist rarefactions carry a helicity deficit

$$\Delta H = \frac{\Phi^2}{2\pi}\int_{-\infty}^{\infty}[q_\infty - q(\zeta)]d\zeta\ . \tag{46}$$

Using the definition of $s(t)$, equation (40) and its governing equation, equation (42), gives the helicity deficit

$$\Delta H = \frac{2\Phi^2 q_\infty v_A}{2\pi}\int_0^\infty [1 - s(t)]dt = \frac{\Phi^2}{2\pi}\,h(\gamma_\infty) = H_{ar} \tag{47}$$

as $t \to \infty$. Thus, the helicity deficit in the pulses equals the helicity added to the coronal magnetic fields. As the flux emerges into the corona, helicity is extracted from the flux tubes. This extraction creates rarefaction pulses, which propagate along the flux tube.

4. DISCUSSION

4.1. *Current Paths*

The foregoing model provides a picture, shown schematically in Figure 6, of how the current from a twisted flux tube passes into the corona after emergence. Recall that the flux tube carries a volume current $I_0 = 2\Phi q_\infty$ on its field lines and an equal return current along its surface. The initial twist suppression, equation (44), indicates that only a fraction $s(0)$ of the tube's volume current passes immediately into the corona [for clarity Fig. 6 depicts a case where $s(0) = 0$, corresponding to instantaneous emergence: $\dot{d} = \infty$]. The remaining fraction, $1 - s(0)$, of the volume current is radially shunted to the tube's surface (see Fig. 6*a*) instead of passing into the corona. The torque from this shunting initiates a plasma rotation, which, along with the twist suppression, forms a torsional Alfvén pulse propagating away from the emergence. The fraction of current shunted, and thus the amplitude of the pulse, depends on the rate of emergence relative to the twist relaxation time $\tau_A = d_0/v_A$.

During emergence, the coronal magnetic field is increasingly twisted by the rotation of its footpoints. The increased coronal twist means that the current entering the corona will increase and the current radially shunted will decrease.

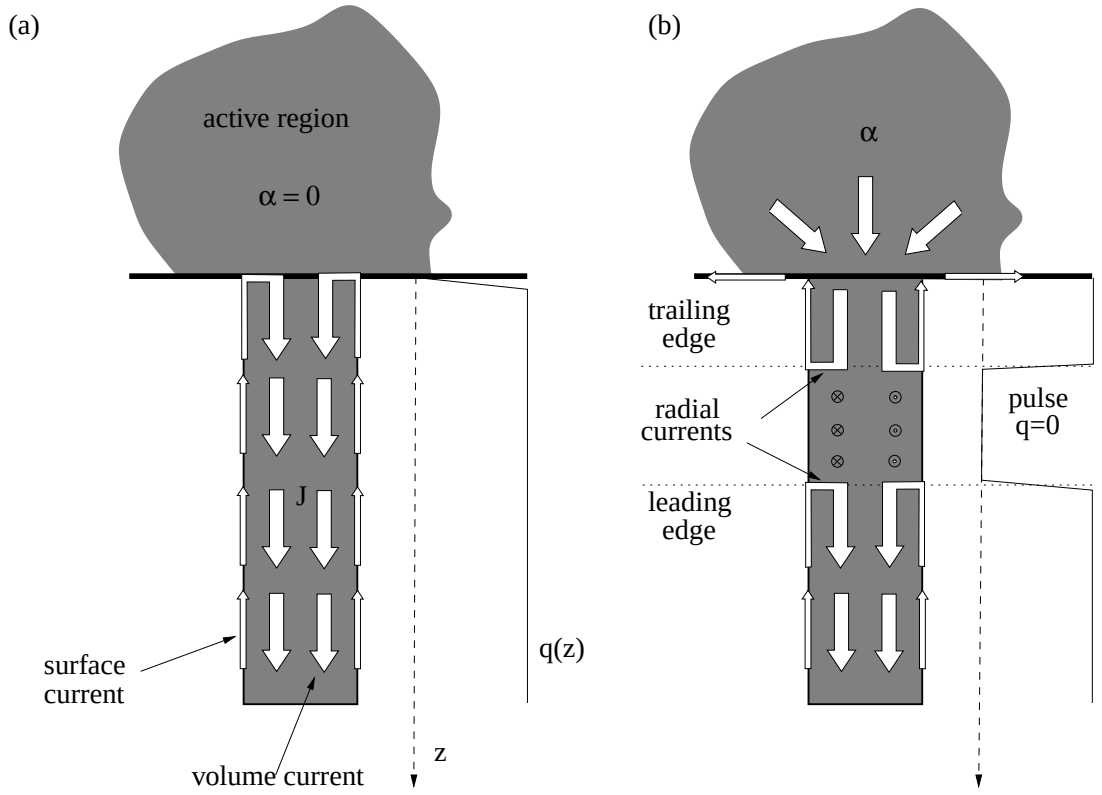

FIG. 6.—Current paths within a torsional Alfvén wave propagating from the corona along a twisted flux tube. The pulse, a twist rarefaction, is launched from the current-free ($\alpha = 0$) corona (*a*). Within the pulse the current is zero ($q = 0$) and the plasma is spinning ($\omega > 0$). Radial currents appear at the leading and trailing edges of the pulse.

In the final state the entire volume current of the flux tube, I_0, will pass into the corona and no current will be shunted. The tube's return current will pass from the surface of the tube onto the layer just beneath the corona known as the merging height (Gabriel 1976). Thus, in our model the final current observed in the active region is equal to the volume current in the twisted flux tube. We find that current within a flux tube can cross field lines but only temporarily.

The introduction mentioned a discrepancy between theory and observations of AR twist; we hoped to explain this discrepancy using our model. The amount of twist observed in AR fields (at the photosphere) is about 1 order of magnitude smaller than two-dimensional theory demands for the integrity of the rising flux tube (Longcope et al. 1999). The present model of emergence does predict a discrepancy of this kind, twist in the coronal field that is smaller than that of the rising tube, even by 1 order of magnitude in cases of rapid emergence. This discrepancy is, however, a temporary state of affairs, and the coronal twist should increase to the tube's value within a few days of emergence. The observational data is a survey of ARs (Pevtsov et al. 1995), which probably measures the asymptotic twist rather than the transient low value. Thus, the emergence model cannot explain the discrepancy and another explanation must be sought.

4.2. *Dynamical Evolution*

The simplest observable prediction of this model is that coronal twist will appear to increase for a period τ_A (about 1 day) after flux emergence. Furthermore, this twist increase will accompany a rotation of the footpoints driven by magnetic forces in the twisted flux tube. The amount by which the coronal current increases depends on the rapidity of the flux emergence. Rapid emergence will result in coronal magnetic flux that is initially quite untwisted. It is expected that these cases will provide the best opportunity to observe the later rise in coronal twist accompanied by photospheric rotation.

The coronal field will change in response to both the AR emergence and the twist of its footpoints. Emergence naturally leads to an expansion of the AR magnetic field, while twisting introduces field-aligned currents that tend to pinch the field. In slow emergence, e.g., Figure 4, the first effect is prevalent and the active region appears to expand throughout. In rapid emergence, Figure 5, the pinching leads to contraction after the region's initial expansion.

In addition to the observable coronal evolution, a twist rarefaction pulse will propagate downward along the flux tube. The source of this rarefaction is the initial helicity deficit in the coronal magnetic field. Because the plasma drains from it, the coronal field is initially stripped of its magnetic helicity. The process of adding helicity to the coronal field creates a deficit in the flux tube; this deficit propagates downward as a torsional Alfvén pulse. Such transport of magnetic helicity into the solar interior might have important consequences for the operation of the solar dynamo (Boozer 1993).

4.3. *Limitations of the Model*

This model is a very crude attempt to join the physics of the convection zone to the physics of the corona. It simplifies the physics of each regime in order to do so. The coronal magnetic field is taken to be fully characterized by its magnetic helicity and the twist α at its footpoints. The

relationship of these quantities is contained in the function $h(\alpha)$. The subphotospheric flux tube serves as a conduit for torsional Alfvén waves. The emerging flux tube transfers helicity into the corona until the footpoint twist, $q(d) = q(-d)$, matches that of the tube.

While the axisymmetric active region we have used is quite unrealistic, it provides a case where $h(\alpha)$ may be calculated. Treating more complicated, three-dimensional active region geometries requires the solution of a free-boundary problem for a constant-α equilibrium, anchored to discrete flux sources and embedded in a potential background. Calculations of this type, which have recently become possible (Chou & Low 1994; Lothian & Browning 1995), can be characterized by new functions $h(\alpha)$. We expect that the general nature of all such functions will be similar to our cylindrical case; $h(\alpha)$ begins at zero and increases monotonically. The most natural scale of variation in h is d^{-1}, the inverse footpoint separation.

The dynamics of the flux tube is modeled by the telegrapher's equations, (22) and (25). These were derived here for straight flux tubes; however, the same equations obtain for general axial geometries (Longcope & Klapper 1997). The most significant complication from a more realistic geometry will come from the variation in v_A along the axis. Wave propagation through variable media is, however, well understood, and such a generalization would not be complicated. Abrupt changes in v_A would obviously reflect some portion of the torsional wave back toward the photosphere, while more gradual variation would generate a low-level reflected component. This might add interesting observable features to the AR's evolution and even provide some insight into the magnetic field strength inside the CZ. In spite of this, we do not expect that the effect will change the basic conclusions of our model.

The AR model and flux tube model are connected across an interface representing the photosphere. Rather than focus on the intricate details of this layer, we have applied global constraints across the layer. We have also shown that this process works for layers of finite thickness as well as for genuine boundaries. In particular, torque about the tube's axis must match across the photosphere since it comes only from magnetic twist and cannot be balanced by pressure gradients. The simplicity of this result was aided by axisymmetry; however, torque is a far more general concept and should apply to flux tubes with more complex internal geometry. We thus expect the general nature of this connection to apply to general magnetic fields.

We thank the anonymous referee for a helpful suggestion on the manuscript. This material is based upon work supported by the National Science Foundation under grant ATM 97-33424 and by NASA under grant NAG5-6110.

APPENDIX

THE CORONAL FIELD

The response of the coronal magnetic field is characterized in terms of the rescaled flux function, $F(x, y)$, which solves equation (34)

$$x \frac{\partial}{\partial x}\left(\frac{1}{x}\frac{\partial F}{\partial x}\right) + \frac{\partial^2 F}{\partial y^2} = -\gamma^2 F\,, \tag{34}$$

inside the interface $x < x_s(y)$. The function is subject to the boundary conditions

$$F(x = 0, y) = 0, \quad \text{I}$$

$$F(x, y = \pm 1) = 1, \quad \text{II}$$

$$F(x = x_s, y) = 1, \quad \text{III}$$

$$\left.\frac{\partial F}{\partial x}\right|_{x = x_s} = 0, \quad \text{IV}\,.$$

While equation (34) appears linear in $F(x, y)$, boundary conditions III and IV introduce nonlinearity owing to their dependence on the solution. For present purposes it is most important to establish that equation (34) has a unique solution for each value γ. The basic results of this paper depend on the existence and general properties of the rescaled helicity function $h(\gamma)$.

We have used two different numerical techniques to solve the free-boundary problem. The functions $F(x, y)$ produced by these very different techniques agree over most of the domain. Most importantly, the rescaled helicity functions,

$$h(\gamma) \equiv 2\gamma \int_{-1}^{1} dy \int_{0}^{x_s(y)} F^2 \frac{dx}{x}\,, \tag{A1}$$

from each technique agree very closely. We used the more robust of these techniques (relaxation) for the figures in the paper. The second technique was developed primarily as a check on the first.

A1. FINITE DIFFERENCE SOLUTION BY RELAXATION

The simplest and most robust technique is based on a method by Wolfson, Vekstein, & Priest (1994). The differential operator from equation (34) is approximated by centered differences on a uniform spatial grid (x_i, y_j)

$$D_{ij}F \equiv \frac{2x_i}{(\Delta x)^2}\left(\frac{F_{i+1,j} - F_{i,j}}{x_{i+1} + x_i} - \frac{F_{i,j} - F_{i-1,j}}{x_i + x_{i-1}}\right) + \frac{F_{i,j+1} - 2F_{i,j} + F_{i,j-1}}{(\Delta y)^2}\,. \tag{A2}$$

At the boundaries, $x_0 = 0$, $x_{Nx} = R$, $y_0 = -y_2$, and $y_{Ny} = 1$, we set $F_{0,j} = 0$, $F_{Nx,j} = 1$, $F_{i,0} = F_{i,2}$, and $F_{i,Ny} = 1$. As long as it remains outside the interface x_s, the specific location of the outer radius R is irrelevant. Values of $F_{i,j}$ in the grid interior are relaxed according to

$$F^{n+1}_{i,j} = F^n_{i,j} - \theta\left[D_{i,j}F^n + g(F^n_{i,j})F^n_{i,j}\right], \tag{A3}$$

where the function $g(F)$

$$g(F) = \begin{cases} \gamma^2, & F \le 1 - 2\delta f \\ \gamma^2 \dfrac{(1-\delta f) - F}{\delta f}, & 1 - 2\delta f < F \le 1 - \delta f \\ 0, & 1 - \delta f < F \end{cases} \tag{A4}$$

divides the AR from the vacuum at the approximate interface where $F = 1 - 1.5\delta f \simeq 1$. Its specific form decreases to zero over a predefined thickness typically chosen to be $\delta f = 10^{-3}$. The parameter θ is chosen to optimize convergence to a solution. To further aid convergence, a solution found on a course grid, say $Nx = Ny = 16$, is then interpolated onto a finer grid. This is then relaxed and interpolated, and relaxed again. The solutions shown, and those used to calculate $h(\gamma)$, were found on $Nx = Ny = 64$ grids.

A2. SERIES SOLUTION

The general solution to equation (34) can be written

$$F(x, y; \gamma) = x\int_0^\infty J_1(kx)\frac{\cosh(y\sqrt{k^2-\gamma^2})}{\cosh(\sqrt{k^2-\gamma^2})}dk + x\sum_{n=0}^{\infty} b_n \cos(yk_n)J_1(x\sqrt{k_n^2-\gamma^2}), \tag{A5}$$

where $k_n = \pi(n + \frac{1}{2})$. The coefficients b_n are arbitrary and will be real if $k_n > \gamma$ and imaginary otherwise. The expression satisfies boundary conditions I and II for all choices of b_n. The free surface x_s is defined by condition III, and the coefficients b_n must be chosen to satisfy condition IV at this interface.

An approximate solution is found by truncating the series at N terms and treating the coefficients $b_1, b_2, \ldots b_N$ as unknowns. Boundary conditions III and IV are satisfied at N axial points $y_1, y_2, \ldots y_N$ lying inside the boundaries $y = 0$ and $y = 1$. At each axial point y_i, the interface location is found by solving the nonlinear equation

$$F(x_{i,s}, y_i) = 1 \tag{A6}$$

for $x_{i,s}$. The radial derivatives at these points constitute N functions of the N unknowns, b_j,

$$\Phi_i(b_j) = \left|\frac{\partial F}{\partial x}\right|_{x_{i,s}, y_i} = 0. \tag{A7}$$

An N-dimensional Newton-Raphson method is used to solve these equations for b_j (Press et al. 1986).

This method has the advantage of treating the exact interface $F = 1$ rather than the approximation $F = 1 - 1.5\delta f$. The interface found this way is slightly outside the approximation from relaxation. Nevertheless, the values of helicity $h(\gamma)$ found both ways agree to within less than 1%.

REFERENCES

Berger, M. A. 1999, in Magnetic Helicity in Space and Laboratory Plasmas, ed. M. R. Brown, R. C. Canfield, & A. A. Pevtsov (Geophys. Monogr. 111; Washington, DC: AGU), 1
Berger, M. A., & Field, G. B. 1984, J. Fluid Mech., 147, 133
Boozer, A. H. 1993, Phys. Fluids B, 5, 2271
Caligari, P., Moreno-Insertis, F., & Schüssler, M. 1995, ApJ, 441, 886
Canfield, R. C., Hudson, H. S., & McKenzie, D. E. 1999, Geophys. Res. Lett., 26, 627
Canfield, R. C., Pevtsov, A. A., & McClymont, A. N. 1996, in ASP Conf. Ser. 111, Magnetic Reconnection in the Solar Atmosphere, ed. R. D. Bentley & J. T. Mariska (San Francisco: ASP), 341
Chou, Y. P., & Low, B. C. 1994, Sol. Phys., 153, 255
Choudhuri, A. R., & Gilman, P. A. 1987, ApJ, 316, 788
Fan, Y., Fisher, G. H., & McClymont, A. N. 1994, ApJ, 436, 907
Finn, J., & Antonsen, T. M., Jr. 1985, Comments Plasma Phys. Controlled Fusion, 9, 111
Fisher, G. H., Chou, D.-Y., & McClymont, A. N. 1989, in Solar System Plasma Physics, ed. J. H. Waite, J. L. Burch, & R. L. Moore (Geophys. Monogr. 54; Washington, DC: AGU), 47
Gabriel, A. H. 1976, Philos. Trans. R. Soc. London, A, 281, 339
Leka, K. D., Canfield, R. C., McClymont, A. N., & van Driel-Gesztelyi, L. 1996, ApJ, 462, 547
Linton, M. G., Longcope, D. W., & Fisher, G. H. 1996, ApJ, 469, 954
Longcope, D. W., Fisher, G. H., & Pevtsov, A. A. 1998, ApJ, 507, 417
Longcope, D. W., & Klapper, I. 1997, ApJ, 488, 443
Longcope, D. W., Linton, M. G., Pevtsov, A. A., Fisher, G. H., & Klapper, I. 1999, in Magnetic Helicity in Space and Laboratory Plasmas, ed. M. R. Brown, R. C. Canfield, & A. A. Pevtsov (Geophys. Monogr. 111; Washington, DC: AGU), 93
Lothian, R. M., & Browning, P. K. 1995, Sol. Phys., 161, 289
Melrose, D. B. 1991, ApJ, 381, 306
———. 1997, ApJ, 486, 521
Moreno-Insertis, F. 1986, A&A, 166, 291
Parker, E. N. 1996, ApJ, 471, 485
Pevtsov, A. A. 2000, ApJ, 531, 553
Pevtsov, A. A., Canfield, R. C., & McClymont, A. N. 1997, ApJ, 481, 973
Pevtsov, A. A., Canfield, R. C., & Metcalf, T. R. 1995, ApJ, 440, L109
Press, W. H., Flannery, B. P., Teukolsky, S. A., & Vetterling, W. T. 1986, Numerical Recipes: The Art of Scientific Computing, (Cambridge: Cambridge Univ. Press)
Priest, E. R. 1982, Solar Magnetohydrodynamics (Geophys. Astrophys. Monogr. 21; Dordrecht: Reidel)
Schüssler, M. 1979, A&A, 71, 79
Spruit, H. C. 1981, A&A, 98, 155
Taylor, J. B. 1974, Phys. Rev. Lett., 33, 1139
Wolfson, R., Vekstein, G. E., & Priest, E. R. 1994, ApJ, 428, 345
Woltjer, L. 1958, Proc. Natl. Acad. Sci., 44, 489